

# Templated growth of covalently bonded three-dimensional carbon nanotube networks originated from graphene

Yifeng Fu<sup>1,2</sup>, Björn Carlberg<sup>1</sup>, Niklas Lindahl<sup>3</sup>, Niclas Lindvall<sup>1</sup>, Johan Bielecki<sup>4</sup>, Aleksandar Matic<sup>4</sup>, Yuxin Song<sup>1</sup>, Zhili Hu<sup>1,5</sup>, Zonghe Lai<sup>1</sup>, Li-Lei Ye<sup>6</sup>, Jie Sun<sup>1</sup>, Yahui Zhang<sup>5</sup>, Yan Zhang<sup>5</sup> and Johan Liu<sup>1,5\*</sup>

<sup>1</sup>Department of Microtechnology and Nanoscience, Chalmers University of Technology, SE-412 96 Göteborg, Sweden

<sup>2</sup>FOAB Elektronik AB, S:t Jörgens väg 8, SE-422 49 Hisings Backa, Sweden

<sup>3</sup>Department of Physics, University of Gothenburg, SE-412 96 Göteborg, Sweden

<sup>4</sup>Department of Applied Physics, Chalmers University of Technology, SE-41296 Göteborg, Sweden

<sup>5</sup>Key Laboratory of Advanced Display and System Applications and SMIT Center, School of Automation and Mechanical Engineering, Box 282, No. 149 Yan Chang Road, Yan Chang Campus, Shanghai University, Shanghai 200072, China

<sup>6</sup>SHT Smart High Tech AB, Fysikgränd 3, SE-412 96 Göteborg, Sweden

\*To whom correspondence should be addressed: Johan Liu, [j.liu@chalmers.se](mailto:j.liu@chalmers.se)

Varieties of applications have been proposed to use carbon nanotubes (CNTs) in different fields such as electronics<sup>1</sup>, photonics<sup>2</sup>, chemistry<sup>3</sup>, biology<sup>4</sup> and their inter-disciplinaries<sup>5-7</sup>. Among them, many applications such as ion separation<sup>8</sup> and thermal interface materials<sup>9</sup> require strong connections between CNTs to realize a specific function. However, the CNTs synthesized by current methods are commonly a sparse material and only weak van der Waals interactions exist between them<sup>10</sup>. Creation of high quality chemical bonding between CNTs remains a formidable challenge in nanotechnology. In this paper, we demonstrate a template-assisted method which enables the growth of covalently bonded CNTs originating from graphene at a large scale. The as-grown CNT networks are suspended over silicon trenches, on which structure atomic force microscopy (AFM) based bending tests are executed. Results show that the Young's modulus of the CNTs is about  $391_{-172}^{+270}$  GPa, which is in accordance with theoretical prediction<sup>11,12</sup> and previous measurement results<sup>13-17</sup> on traditionally-synthesized CNTs. It is also observed that the covalently bonded CNT structure can effectively distribute external loading throughout the network to improve the mechanical strength. This covalently bonded three-dimensional CNT network provides great opportunities to the application of CNTs in complex device fabrication<sup>18-20</sup>, energy storage<sup>21,22</sup>, ion/molecule separation<sup>8,23</sup>, thermal interface material development<sup>9,24</sup>, etc.

CNT is a one dimensional material which has attracted tremendous research interest due to the exceptional electrical<sup>25,26</sup>, thermal<sup>27-30</sup> and mechanical<sup>11-17</sup> properties in the longitudinal direction. The CNTs in these investigations appear in three different manners, namely single CNTs for nano/micro device fabrication<sup>31,32</sup>, CNT bundles for component integration<sup>33,34</sup> and CNT networks<sup>35,36</sup> to extend the excellent properties into two or three dimensions. Up to date,

the synthesis of single CNTs and CNT bundles is becoming mature by chemical vapor deposition (CVD) method. While the CNT networks can be produced by laser ablation<sup>37,38</sup> and arc discharge<sup>39,40</sup> techniques, or obtained by post-growth processing of CVD-deposited aligned CNT films<sup>41,42</sup>. However, the CNT network produced by either of the above methods is commonly a sparse material, in which the CNTs just physically contact with each other and van der Waals force is the only interaction between them<sup>10</sup>. The weak interaction prevents the CNTs talking to each other therefore leading to low resistance against sliding<sup>10</sup>, and producing huge electrical and thermal contact resistance among CNTs<sup>43</sup>. This will not only restrict the application spectrum of CNTs but also greatly lower the performance of the CNT-based components. Therefore, a few methods are developed to build up covalent inter-tube bonding in the network. The first route is introducing inter-tube connections by post-growth processing. Since carbon atoms in CNTs can be activated by irradiation<sup>44</sup>, electron<sup>10,45</sup> or ion<sup>46,47</sup> beams were applied to first amorphize two adjacent CNT surfaces and then re-construct the carbon atoms to generate covalent bonding between these two CNTs. However, the high irradiation applied in this process resulted in degradation of the structure around the contact region<sup>48</sup>, which consequently lowers the performance of CNTs. Furthermore, this method is favorable for making devices/structures at a small scale, and it is very unlikely scalable for volume production. The second route is growing the CNT network in a special way, following a pre-defined template or introducing additives into the growth/annealing process. The aluminium-templated growth method developed by Li J et al.<sup>49</sup> successfully produced Y-junctions in CNTs, in which a large-diameter CNT can be branched into two smaller ones. However, limited by the shape of the template, there is no connection between those large-diameter CNTs so the inter-connection is not propagated throughout the material. Additives such as sulfur<sup>50,51</sup> and boron<sup>52</sup> were also introduced into the

CNT growth or annealing process, and covalent bonding between CNTs was created. However, these additives can bring impurities and defects<sup>52</sup> into the CNTs which are detrimental to the performance. Branched CNTs were also produced by adjusting the growth conditions such as gas flow<sup>53</sup> and magnetic field<sup>54</sup> in the CVD process, where catalyst particles were re-assembled therefore CNTs were grown in a branched manner. Similar to Li's work<sup>49</sup>, these branched CNTs can be excellent candidate for multi-terminal electronic devices, but they could not extend the outstanding properties of CNTs into three dimensions in a network. Inter-connected CNT structures were also found in a normal typical arc discharge or CVD process occasionally<sup>55,56</sup>, but the mechanism of formation remains unidentified.

In this paper, we report a new strategy to grow covalently bonded CNTs which is scalable for mass production. These CNTs are grown on a cross-linked three-dimensional nickel (Ni) template by CVD method. Different from the traditional particle-catalyzed CVD method<sup>57</sup> for CNT growth, we grow graphene layers on a continuous cylindrical Ni surface<sup>58</sup> to form tubular structures, i.e. CNTs. After the Ni template core is etched away, the inter-connected CNT networks are obtained. A schematic of the CNT network is shown in Fig. 1, in which covalent inter-tube bondings are created.

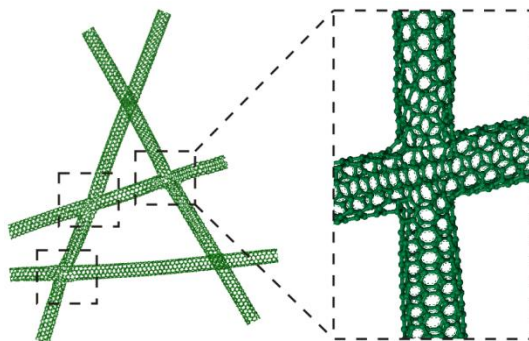


Figure 1 Schematic of a covalently bonded CNT network.

The synthesis process of the covalently bonded CNT network is illustrated in Fig. 2. The experiment starts with the electrospinning of polyvinyl butyral (PVB) and nickel nitrate hexahydrate ( $\text{Ni}(\text{NO}_3)_2 \cdot 6\text{H}_2\text{O}$ ) dissolved ethanol solution, as shown in Fig. 2a. The electrospun nanofiber network which consists of PVB and  $\text{Ni}(\text{NO}_3)_2$  was collected on a conductive aluminum foil. Since wet  $\text{Ni}(\text{NO}_3)_2$  containing PVB fibers sprayed from the syringe can easily fuse to each other, large amounts of inter-connections throughout the nanofiber network can be created, as marked by dashed frames in Fig. 2b. In addition, electrospinning is a facilely scalable and well controllable technique. Therefore it is easy to deposit such nanofiber networks to large thickness to obtain three dimensional structures. The nanofiber network was then peeled off from the aluminum foil and annealed in oxygen ( $\text{O}_2$ ) at  $400\text{ }^\circ\text{C}$  for 2 hours, thereby removing PVB from the fibers and decomposing  $\text{Ni}(\text{NO}_3)_2$  to  $\text{NiO}_x$ , as displayed in Fig. 2c. Afterwards, the  $\text{NiO}_x$  fiber network was moved into a commercial graphene/CNT growth system (Black Magic II, Aixtron) and heated up to  $400\text{ }^\circ\text{C}$  in hydrogen ( $\text{H}_2$ ) environment. The reduction process lasted for 2 hours, whereby a pure Ni fiber network was obtained (shown in Fig. 2d). After elevating the temperature up to  $750\text{ }^\circ\text{C}$  and annealing the Ni fibers for 5 minutes, argon (Ar) diluted acetylene ( $\text{C}_2\text{H}_2$ ) was introduced into the system to start the graphene growth on the cylindrical surfaces of the inter-connected Ni fibers, as shown in Fig. 2e. Since in this case the growth of graphene has to follow the morphology of the Ni template, the inter-connected graphene-tube, i.e. CNT, structure was formed. In order to harvest the inter-connected CNTs, the graphene shells covered Ni fiber network was immersed into an iron chloride ( $\text{FeCl}_3$ ) solution to etch away the Ni core. Consequently, the covalently bonded three dimensional CNT network was produced as sketched in Fig. 2f.

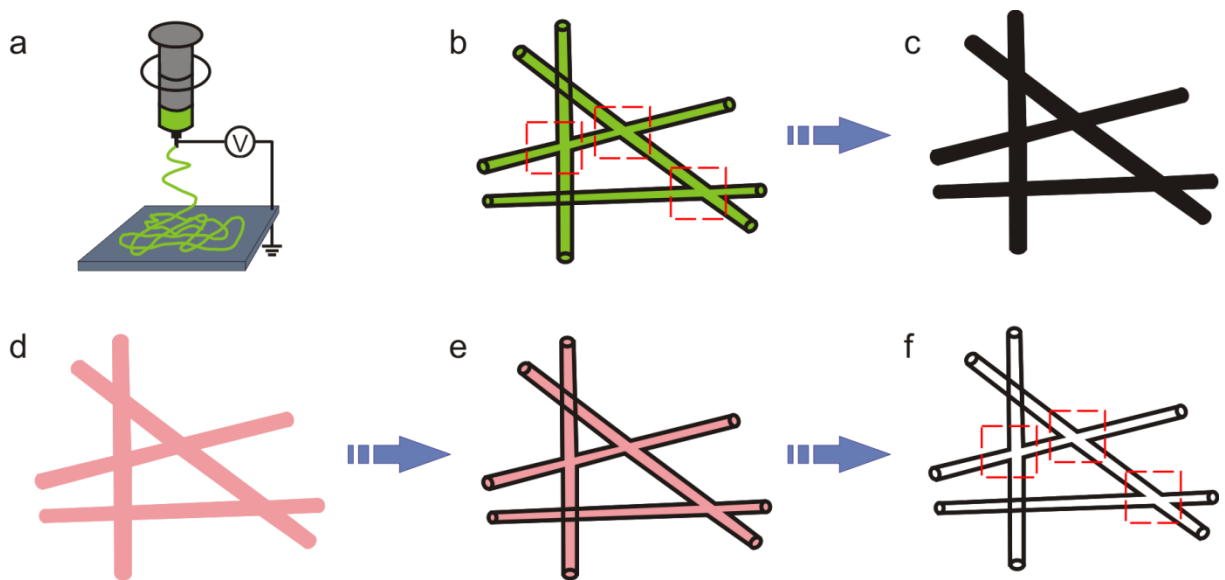


Figure 2 Synthesis flow chart of the covalently bonded three dimensional CNT networks. a, Electrospinning of  $\text{Ni}(\text{NO}_3)_2$  contained PVB nanofiber networks. b, Inter-connected electrospun  $\text{Ni}(\text{NO}_3)_2/\text{PVB}$  nanofibers in the network. The fused inter-connection joints are marked by dashed frames. c,  $\text{NiO}_x$  nanofiber network after the burning of PVB and decomposition of  $\text{Ni}(\text{NO}_3)_2$  in  $\text{O}_2$ . d, Pure Ni fiber network reduced from  $\text{NiO}_x$  by  $\text{H}_2$ , acting as graphene-tube growth template. e, Graphitic layer growth on the inter-connected three dimensional Ni template. f, Chemical etching of Ni core in  $\text{FeCl}_3$  solution so that covalently bonded three dimensional CNT network is obtained. The inter-connection joints are marked by dashed frames.

The electrospun  $\text{Ni}(\text{NO}_3)_2$  contained PVB nanofiber network is shown in Fig. S1, from which it can be seen that the nanofibers are inter-connected with each other throughout the network structure. A locally enlarged typical inter-connection joint is shown in Fig. 3a. Making the nanofiber network thicker with longer time for electrospinning deposition, this inter-connected structure can easily be extended into three dimensions. Fig. 3b and Fig. S2 shows the pure Ni

fibers which are reduced from  $\text{NiO}_x$ . It can be clearly observed that the inter-connected three dimensional structure is retained after the thermal decomposition process in  $\text{O}_2$  (Fig. 2c) and the reduction process in  $\text{H}_2$  (Fig. 2d). The reduced Ni fibers were characterized by X-ray diffraction (XRD), the diffraction pattern is displayed in Fig. 3c. The peaks in the XRD pattern show a high purity of Ni but also the existence of NiO in the sample. This small amount of NiO originates from the oxidation of Ni fibers exposed to air during the XRD characterization. Energy-dispersive X-ray spectroscopy (EDX) pattern in Fig. S3 further confirms the metallic Ni fibers. Once pure Ni fibers were acquired, they were annealed at  $750\text{ }^\circ\text{C}$  for 5 minutes.  $\text{C}_2\text{H}_2$  was then introduced to start the graphene growth on the Ni surface. Fig. 3d shows the Ni fibers after graphene growth. Transmission electron microscopy (TEM) image (Fig. 3e) shows that well crystallized graphene layers have been grown on the Ni fibers with an inter-layer distance of about 0.34 nm. The multi-layer graphene covered Ni fiber network was then immersed into 30 wt% of  $\text{FeCl}_3$  solution to remove the Ni template. The CNT network was herein harvested and is shown in Fig. 3f. More detailed inter-connected CNT structures are available in Fig. S4. The TEM images in Fig. 3g clearly show a multi-branched joint where CNTs are internally connected to each other. A broken CNT perpendicular to the paper plane at the right lower corner even allows us to look inside to the inter-connected CNT structure. A schematic in Fig. 3g illustrates the three dimensional structure of this CNT network. The  $sp^2$  hybridized carbon structure in this material was confirmed by Raman spectroscopy. The three most intense peaks in Fig. 3h located at  $1357\text{ cm}^{-1}$ ,  $1578\text{ cm}^{-1}$  and  $2702\text{ cm}^{-1}$  represent the D, G and 2D modes respectively. The relatively low D peak suggests a high quality of  $sp^2$  bonding in the material<sup>59</sup>.

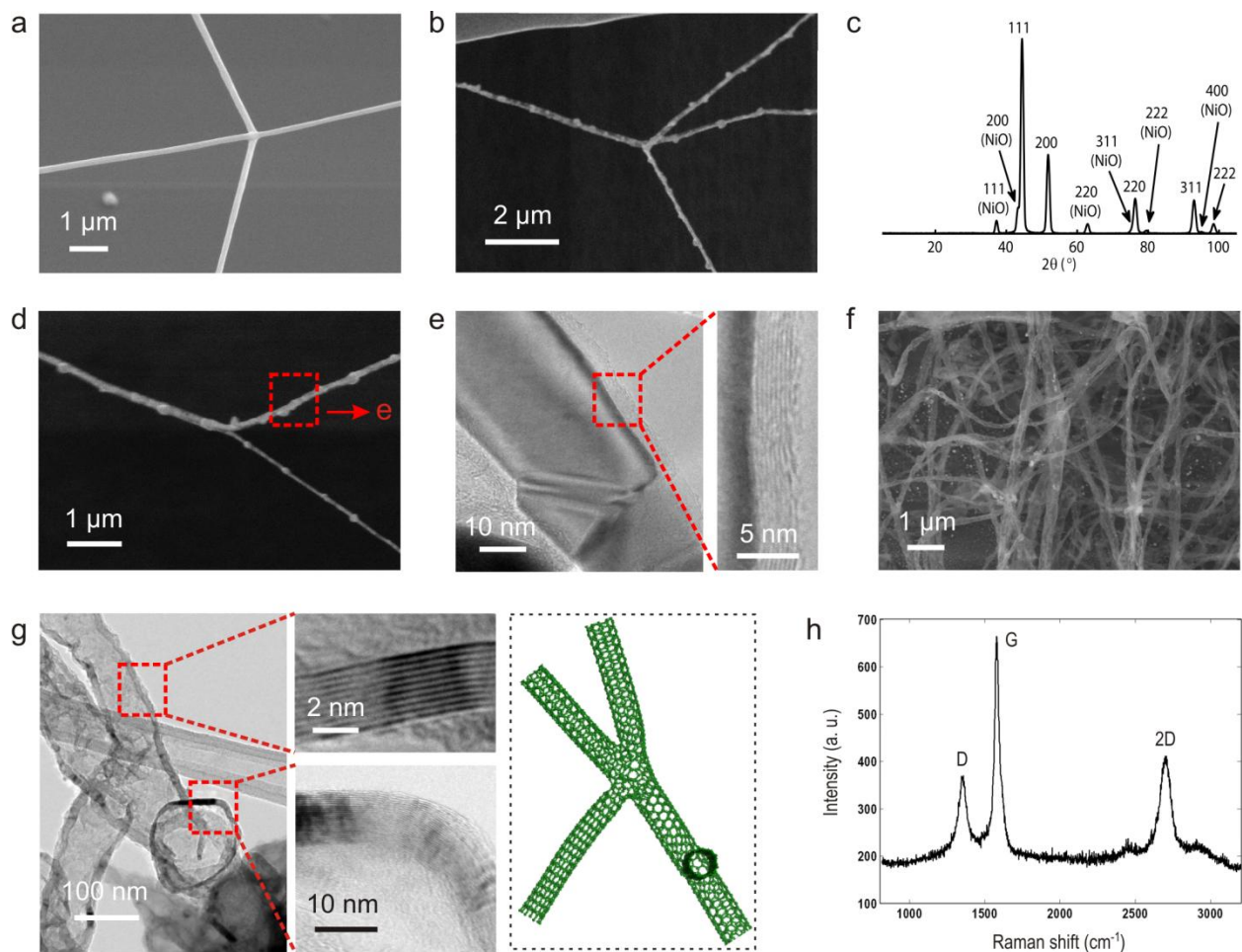


Figure 3 Fabrication and characterization of the covalently bonded CNT network. a, Inter-connected  $\text{Ni}(\text{NO}_3)_2$  contained PVB nanofibers produced by electrospinning. b,  $\text{H}_2$  reduced inter-connected Ni fibers. It can be seen that the three dimensional structure is retained after the thermal decomposition process in  $\text{O}_2$  and reduction process in  $\text{H}_2$ . c, XRD pattern of the  $\text{H}_2$  reduced Ni fibers. Ni is identified by the most intense peaks. The small amount of NiO was from the oxidation of Ni when it was exposed to air during XRD characterization. d, Inter-connected Ni fibers with graphene layers grown on the cylindrical surfaces. e, Well crystallized graphene layers on the Ni fiber surface. f, Harvested CNT network after removing Ni template by chemical etching in  $\text{FeCl}_3$  solution. g, Covalently bonded, internally connected CNT multi-branched structure. The broken CNT at the right lower corner allows us to look inside to the

CNT structure. h, Raman spectrum of the harvested material. D, G and 2D peaks are located at  $1357\text{ cm}^{-1}$ ,  $1578\text{ cm}^{-1}$  and  $2702\text{ cm}^{-1}$  respectively. Relatively low D peak indicates a high quality  $sp^2$  hybridized carbon structure in the material.

In order to examine the as-fabricated CNTs, atomic force microscopy (AFM) assisted bending tests were performed on both suspended single CNTs and suspended CNT networks. The test structure and principle are schematically shown in Fig. 4a, where a loading is applied at the midspan of the suspended CNT via an AFM tip. To suspend the CNTs,  $\text{Ni}(\text{NO}_3)_2$  contained PVB nanofibers were electrospun and collected on trenched silicon chips, then following thermal decomposition, reduction, graphene growth and template etching processes were kept the same as described above. More details about the suspension of CNTs are available in Fig. S5. A Ntegra Aura AFM with a NSG-10 cantilever was used for the bending test. The spring constant of the cantilever was measured to be  $12.3\text{ N/m}$ . To find the position of the suspended CNTs, the sample was scanned by the AFM in tapping mode. The suspended single CNT and the interconnected CNT network were found as shown in Fig. 4b and Fig. 4c. During the bending test, the AFM tip oscillation was turned off. The deflection of the cantilever and the displacement of the piezo in the AFM were recorded simultaneously, as shown in Fig. S6. The force-deflection curves of the tested single CNT and the CNT in a network are displayed in Fig. 4d. Repeated tests at different positions close to each other on the CNTs demonstrated the robustness of the results, see Fig. S6. Assuming the force loaded on the individual CNT is  $F$ , the deflection of the CNT is  $\delta$  and the span of the suspended CNT is  $l$ , the force-deflection relation of the tested CNT can be herein expressed as<sup>60</sup>:

$$F = \frac{192 \cdot E \cdot I}{l^3} \cdot \delta \quad (1)$$

where  $E$  is Young's modulus of the CNT, and  $I$  is the second area moment on the cross section of the CNT. Correlated with the approximately linear force-deflection curve of the individual CNT in Fig. 4d, Young's modulus of the as-grown CNT is extracted to be  $391_{-172}^{+270}$  GPa. The large bounds of modulus originate from the difficulty to measure the inner diameter of the CNT. More detailed discussion on determining the inner diameter is presented in the supplementary information. The extracted Young's modulus is in agreement with the previous theoretical prediction<sup>11,12</sup> and experimental measurements<sup>13-17</sup> on a single CNT grown by the traditional methods. More details about the mechanical test procedure and calculation of the Young's modulus are also available in the supplementary information.

Fig. 4d also reveals that a CNT in the network can withstand much higher loading force than the individual suspended CNT under the same deflection. For instance, the same deflection of 200 nm is triggered by 8 nN loading on the individual CNT compared to 78 nN loading on the CNT in a network. This is consistent with previous experimental and modeling results<sup>61</sup> on cross-linked fibrin fibers which have similar network structure, i.e. the cross-linked structure can distribute external loading throughout the network to avoid a concentrated stress and failure so that effectively improve the mechanical strength of the network.

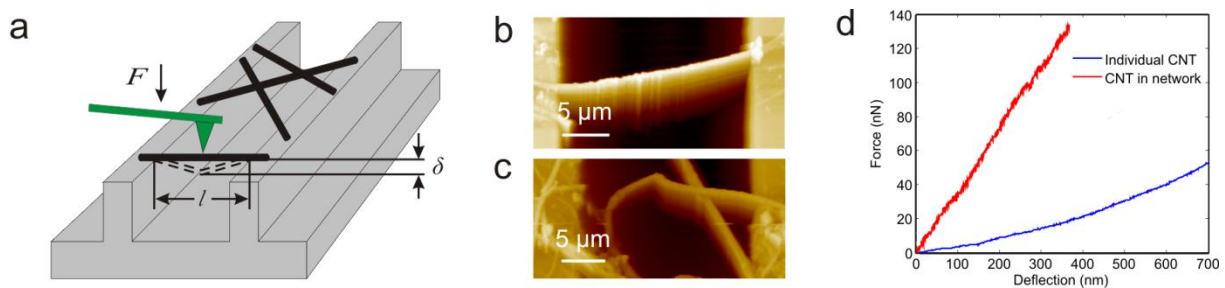


Figure 4 Mechanical tests on the individually suspended CNT and the inter-connected CNT network. a, Schematic of the test structure and principle.  $F$  is the force loaded at the midspan of the single CNT,  $\delta$  is deflection of the CNT and  $l$  is the span of the CNT. b and c, AFM image of the individually suspended CNT and the suspended CNT network, respectively. d, Approximately linear force-deflection curves of the individual CNT and the CNT in the network, obtained from the mechanical tests.

$\text{Cu}(\text{NO}_3)_2$  was also dissolved in ethanol solution together with PVB and electrospun into nanofiber networks. Using the same fabrication process as described above for  $\text{Ni}(\text{NO}_3)_2$  contained PVB fibers, pure Cu nanofiber networks were produced.  $\text{C}_2\text{H}_2$  was also utilized as carbon precursor to grow graphene on the inter-connected Cu template. However, most of the Cu fibers melted into discrete islands during the growth even at a comparably low temperature of about  $700\text{ }^\circ\text{C}$  (see Fig. S7). Similar phenomenon on Cu nano wires was also observed at higher temperature in an earlier report<sup>58</sup>.

In summary, we have demonstrated a new method to grow covalently bonded CNT networks. Different from traditional particle-catalyzed methods, these CNTs are grown in the same way as graphene. Since the Ni nanofibers in the template are inter-connected with each other forming a network structure, the as-grown CNTs are covalently bonded throughout the network. In

addition, the Ni template is easy to produce in large volume by the electrospinning-based technique, therefore the covalently bonded CNTs can extend their excellent properties from the longitudinal direction to three dimensions at a macro scale. AFM based mechanical tests on the suspended individual CNTs show that the Young's modulus of the as-grown CNTs is about  $391_{-172}^{+270}$  GPa, which is in accordance with the theoretical expectation and agrees with previous experimental measurements on traditionally grown CNTs. The Raman spectra together with the mechanical tests reveal the high quality of the synthesized CNTs. In contrast to individual CNTs, the covalently bonded CNT structure can effectively distribute stress throughout the network to improve the mechanical strength of the material. This three-dimensional CNT network offers new opportunities for device design and material development where the covalent bonding between CNTs is essential but remains a big challenge.

## Methods

**Preparation and confirmation of inter-connected Ni template.** The fabrication of Ni template starts with the preparation of electrospinning solution. Typically 25 wt% of  $\text{Ni}(\text{NO}_3)_2 \cdot 6\text{H}_2\text{O}$  and 5 wt% of PVB dissolved in ethanol was prepared. The electrospinning was performed by applying 15 kV with an electrode-to-collector distance of 12 cm at ~50% relative humidity at room temperature. The  $\text{Ni}(\text{NO}_3)_2$  contained PVB fiber network was collected on an aluminum foil and peeled off for thermal decomposition in  $\text{O}_2$  flow (3 l/min) at 400 °C for 2 hours. Therefore PVB was burned out and  $\text{Ni}(\text{NO}_3)_2$  was decomposed into  $\text{NiO}_x$ . The  $\text{NiO}_x$  nanofibers were moved into a commercial graphene/CNT growth system (Black Magic II, Aixtron) and reduced in  $\text{H}_2$  with a flow rate of 20 standard cubic centimeter per minute (sccm) at 400 °C. The

reduction process lasted for 2 hours. The reduced fibers are shown in Fig. 3b and Fig. S2. XRD (X'Pert Materials Research Diffractometer, Philips) was used to confirm the formation of metallic Ni fibers following the reduction process. A Cu-K $\alpha$  X-ray source at 45 kV and 40 mA was utilized. A wide range scan ( $2\theta$  range 5–105  $^\circ$ ) was carried out utilizing a fixed diffraction slit with Ni filter as primary optics, and a parallel beam collimator with proportional detector was used as diffracted optics. The signal background was manually subtracted. EDX was performed in the TEM (Tecnai T20 FEI) under 200 keV.

**Growth of graphene layers.** Once NiO $_x$  was reduced into pure Ni fibers, 1000 sccm argon (Ar) flow was introduced into the growth system and the temperature was elevated up to 750  $^\circ$ C to anneal the Ni fibers. After 5 minutes annealing, 10 sccm C $_2$ H $_2$  was pumped in to start the graphene growth on the Ni fiber surfaces. The growth lasted for 30 seconds. After the growth, the samples were cooled down to room temperature at 200  $^\circ$ C/min in H $_2$  and Ar environment.

**Microscopic characterization of inter-connected CNTs.** The graphene shells covered Ni fiber network was immersed into 30 wt% FeCl $_3$  solution for 15 hours to etch away the Ni template. The floating CNT network was then transferred onto a carbon-deposited Cu grid for SEM (Zeiss Supra 60 VP) and TEM (Tecnai T20 FEI) observation. The samples were dried in an acetone-contained critical point dryer to prevent damaging the CNT structure from capillary force. The  $sp^2$  carbon structure was confirmed by Raman spectroscopy. Unpolarized Raman spectra were collected with a Dilor-XY800 spectrometer using a liquid-nitrogen cooled CCD detector. A single grating configuration with a focal distance of 30 cm and 200  $\mu$ m slit width gave a spectral resolution of 4  $cm^{-1}$  with a 1500  $cm^{-1}$  spectral window. A holographic notch filter was used to suppress the contribution from the laser line. The horizontally polarized 514 nm line from an Ar $^+$  laser excited the sample through a 100x micro-objective with a spot size of  $\sim$ 1  $\mu$ m. The laser

power was kept below 4 mW to avoid sample damage. An accumulation time of 10 min was used for the individual spectra and the average of three such spectra was used in order to minimize noise.

**Mechanical tests on suspended CNTs.** First, the  $\text{Ni}(\text{NO}_3)_2$  contained PVB fibers were deposited on trenched silicon chips. Therefore, a suspended inter-connected fiber network was obtained on the chips, as shown in Fig. S5. The trenches on the chips were fabricated by standard photolithography and deep reactive ion etching (DRIE) processes. The following processes including thermal decomposition, reduction, graphene growth and template etching were kept the same as described above. Finally, the inter-connected CNT network was suspended on the trenches. A Ntegra Aura AFM with a NSG-10 cantilever was used for the mechanical test. The spring constant of the cantilever was measured to ensure precise bending tests on the CNTs. More details about the calibration of the cantilever are available in the supplementary information. During the bending tests, both the cantilever and the CNT were deflected. The force exerted by the tip was obtained from the deflection of the cantilever. The deflection of the CNT was calculated by subtracting the deflection of the cantilever from the total displacement of the piezo in the AFM. The deflection of CNT was plotted against the exerted force from the tip, as shown in Fig. 4d.

## References

1. Tans, S.J., Verschueren, A.R.M. & Dekker, C. Room-temperature transistor based on a single carbon nanotube. *Nature* **393**, 49-52 (1998).

2. Barone, P.W., Baik, S., Heller, D.A. & Strano, M.S. Near-infrared optical sensors based on single-walled carbon nanotubes. *Nature Mater.* **4**, 86-92 (2005).
3. Wong, S.S., Joselevich, E., Woolley, A.T., Cheung, C.L. & Lieber, C.M. Covalently functionalized nanotubes as nanometre- sized probes in chemistry and biology. *Nature* **394**, 52-55 (1998).
4. Williams, K.A., Veenhuizen, P.T.M., de la Torre, B.G., Eritja, R. & Dekker, C. Nanotechnology: Carbon nanotubes with DNA recognition. *Nature* **420**, 761 (2002).
5. Aliev, A.E. et al. Giant-stroke, superelastic carbon nanotube aerogel muscles. *Science* **323**, 1575-1578 (2009).
6. Hinds, B.J. et al. Aligned multiwalled carbon nanotube membranes. *Science* **303**, 62-65 (2004).
7. Richard, C., Balavoine, F., Schultz, P., Ebbesen, T.W. & Mioskowski, C. Supramolecular self-assembly of lipid derivatives on carbon nanotubes. *Science* **300**, 775-778 (2003).
8. Park, J.H., Sinnott, S.B. & Aluru, N.R. Ion separation using a Y-junction carbon nanotube. *Nanotechnology* **17**, 895-900 (2006).
9. Bozlar, M. et al. Carbon nanotube microarchitectures for enhanced thermal conduction at ultralow mass fraction in polymer composites. *Adv. Mater.* **22**, 1654-1658 (2010).
10. Kis, A. et al. Reinforcement of single-walled carbon nanotube bundles by intertube bridging. *Nature Mater.* **3**, 153-157 (2004).
11. Lu, J.P. Elastic properties of carbon nanotubes and nanoropes. *Phys. Rev. Lett.* **79**, 1297 (1997).
12. Hernandez, E., Goze C., Bernier, P, & Rubio A. Elastic properties of C and  $B_xC_yN_z$  composite nanotubes. *Phys. Rev. Lett.* **80**, 4502-4505 (1998).

13. Jacobsen, R.L., Tritt, T.M., Guth, J.R., Ehrlich, A.C. & Gillespie D.J. Mechanical properties of vapor-grown carbon fiber. *Carbon* **33**, 1217-1221 (1995).
14. Wong, E.W., Sheehan, P.E. & Lieber, C.M. Nanobeam mechanics: Elasticity, strength, and toughness of nanorods and nanotubes. *Science* **277**, 1971-1975 (1997).
15. Yu, M.-F. et al. Strength and breaking mechanism of multiwalled carbon nanotubes under tensile load. *Science* **287**, 637-640 (2000).
16. Demczyk, B. et al. Direct mechanical measurement of the tensile strength and elastic modulus of multiwalled carbon nanotubes. *Mater. Sci. Eng. A* **334**, 173-178 (2002).
17. Kim, G.T., Gu, G., Waizmann, U. & Roth, S. Simple method to prepare individual suspended nanofibers. *Appl. Phys. Lett.* **80**, 1815 (2002).
18. Xu, H. The logical choice for electronics?. *Nature Mater.* **4**, 649-650 (2005).
19. Papadopoulos, C., Rakitin, A., Li, J., Vedenev, A.S. & Xu, J.M. Electronic transport in Y-junction carbon nanotubes. *Phys. Rev. Lett.* **85**, 3476 (2000).
20. Bandaru, P.R., Daraio, C., Jin, S. & Rao, A.M. Novel electrical switching behaviour and logic in carbon nanotube Y-junctions. *Nature Mater.* **4**, 663-666 (2005).
21. Che, G., Lakshmi, B.B., Fisher, E.R. & Martin, C.R. Carbon nanotubule membranes for electrochemical energy storage and production. *Nature* **393**, 346-349 (1998).
22. Assfour, B., Leoni, S., Seifert, G. & Baburin, I.A. Packings of carbon nanotubes - New materials for hydrogen storage. *Adv. Mater.* **23**, 1237-1241 (2011).
23. Noy, A. et al. Nanofluidics in carbon nanotubes. *Nano Today* **2**, 22-29 (2007).
24. Lin, W., Moon, K. & Wong, C.P. A combined process of in situ functionalization and microwave treatment to achieve ultrasmall thermal expansion of aligned carbon nanotube-

- polymer nanocomposites: toward applications as thermal interface materials. *Adv. Mater.* **21**, 2421-2424 (2009).
25. Frank, S., Poncharal, P., Wang, Z.L. & Heer, W.A. de Carbon nanotube quantum resistors. *Science* **280**, 1744-1746 (1998).
26. Wei, B.Q., Vajtai, R. & Ajayan, P.M. Reliability and current carrying capacity of carbon nanotubes. *Appl. Phys. Lett.* **79**, 1172-1174 (2001).
27. Berber, S. Unusually high thermal conductivity of carbon nanotubes. *Phys. Rev. Lett.* **84**, 4613-4616 (2000).
28. Kim, P., Shi, L., Majumdar, A. & McEuen, P.L. Thermal transport measurements of individual multiwalled nanotubes. *Phys. Rev. Lett.* **87**, 215502 (2001).
29. Fujii, M. Measuring the thermal conductivity of a single carbon nanotube. *Phys. Rev. Lett.* **95**, (2005).
30. Li, Q., Liu, C., Wang, X. & Fan, S. Measuring the thermal conductivity of individual carbon nanotubes by the Raman shift method. *Nanotechnology* **20**, 145702 (2009).
31. Jang, J.E. et al. Nanoelectromechanical switches with vertically aligned carbon nanotubes. *Appl. Phys. Lett.* **87**, 163114 (2005).
32. Kaul, A.B., Wong, E.W., Epp, L. & Hunt, B.D. Electromechanical Carbon Nanotube Switches for High-Frequency Applications. *Nano Lett.* **6**, 942-947 (2006).
33. De Heer, W.A., Chatelain, A. & Ugarte, D. A carbon nanotube field-emission electron source. *Science* **270**, 1179-1180 (1995).
34. Wang, T., Jeppson, K., Olofsson, N., Campbell, E.E.B. & Liu, J. Through silicon vias filled with planarized carbon nanotube bundles. *Nanotechnology* **20**, 485203 (2009).

35. Kaempgen, M., Chan, C.K., Ma, J., Cui, Y. & Gruner, G. Printable thin film supercapacitors using single-walled carbon nanotubes. *Nano Lett.* **9**, 1872-1876 (2009).
36. Topinka, M.A. et al. Charge transport in interpenetrating networks of semiconducting and metallic carbon nanotubes. *Nano Lett.* **9**, 1866-1871 (2009).
37. Yudasaka, M. et al. Mechanism of the effect of NiCo, Ni and Co catalysts on the yield of single-wall carbon nanotubes formed by pulsed Nd:YAG laser ablation. *J. Phys. Chem. B* **103**, 6224-6229 (1999).
38. Scott, C.D., Arepalli, S., Nikolaev, P. & Smalley, R.E. Growth mechanisms for single-wall carbon nanotubes in a laser-ablation process. *Appl. Phys. A* **72**, 573-580 (2001).
39. Shi, Z. et al. Mass-production of single-wall carbon nanotubes by arc discharge method. *Carbon* **37**, 1449-1453 (1999).
40. Kiselev, N.A. et al. Double-walled carbon nanotubes fabricated by a hydrogen arc discharge method. *Carbon* **39**, 761-770 (2001).
41. Meitl, M.A. et al. Solution casting and transfer printing single-walled carbon nanotube films. *Nano Lett.* **4**, 1643-1647 (2004).
42. Tawfik, S., O'Brien, K. & Hart, A.J. Flexible High-conductivity carbon-nanotube interconnects made by rolling and printing. *Small* **5**, 2467-2473 (2009).
43. Nirmalraj, P.N., Lyons, P.E., De, S., Coleman, J.N. & Boland, J.J. Electrical connectivity in single-walled carbon nanotube networks. *Nano Lett.* **9**, 3890-3895 (2009).
44. Banhart, F. Irradiation effects in carbon nanostructures. *Rep. Prog. Phys.* **62**, 1181-1221 (1999).
45. Terrones, M., Terrones, H., Banhart, F., Charlier, J.-C. & Ajayan, P.M. Coalescence of single-walled carbon nanotubes. *Science* **288**, 1226-1229 (2000).

46. Stahl, H., Appenzeller, J., Martel, R., Avouris, P. & Lengeler, B. Intertube coupling in ropes of single-wall carbon nanotubes. *Phys. Rev. Lett.* **85**, 5186 (2000).
47. Terrones, M. et al. Molecular junctions by joining single-walled carbon nanotubes. *Phys. Rev. Lett.* **89**, 075505 (2002).
48. Krasheninnikov, A., Nordlund, K., Keinonen, J. & Banhart, F. Ion-irradiation-induced welding of carbon nanotubes. *Phys. Rev. B* **66**, (2002).
49. Li, J., Papadopoulos, C. & Xu, J. Nanoelectronics: Growing Y-junction carbon nanotubes. *Nature* **402**, 253-254 (1999).
50. Romo-Herrera, J.M. et al. An atomistic branching mechanism for carbon nanotubes: sulfur as the triggering agent. *Angew. Chem. Int. Ed.* **47**, 2948-2953 (2008).
51. Romo-Herrera, J.M. et al. The role of sulfur in the synthesis of novel carbon morphologies: from covalent Y-junctions to sea-urchin-like structures. *Adv. Funct. Mater.* **19**, 1193-1199 (2009).
52. Endo, M. et al. Atomic nanotube welders: boron interstitials triggering connections in double-walled carbon nanotubes. *Nano Lett.* **5**, 1099-1105 (2005).
53. Wei, D. et al. A new method to synthesize complicated multibranch carbon nanotubes with controlled architecture and composition. *Nano Lett.* **6**, 186-192 (2006).
54. Wei, D. et al. A magnetism-assisted chemical vapor deposition method to produce branched or iron-encapsulated carbon nanotubes. *J. Am. Chem. Soc.* **129**, 7364-7368 (2007).
55. Ting, J.-M. & Chang, C.-C. Multijunction carbon nanotube network. *Appl. Phys. Lett.* **80**, 324 (2002).
56. Liu, Q., Liu, W., Cui, Z.-M., Song, W.-G. & Wan, L.-J. Synthesis and characterization of 3D double branched K junction carbon nanotubes and nanorods. *Carbon* **45**, 268-273 (2007).

57. Jeong, G., Olofsson, N., Falk, L., & Campbell, E. Effect of catalyst pattern geometry on the growth of vertically aligned carbon nanotube arrays. *Carbon* **47**, 696-704 (2009).
58. Wang, R., Hao, Y., Wang, Z., Gong, H. & Thong, J.T.L. Large-diameter graphene nanotubes synthesized using Ni nanowire templates. *Nano Lett.* **10**, 4844-4850 (2010).
59. Ferrari, A.C. et al. Raman spectrum of graphene and graphene layers. *Phys. Rev. Lett.* **97**, 187401 (2006).
60. Gere, J.M. & Timoshenko, S.P. *Mechanics of Materials*. (Pws Pub Co: 1997).
61. Hudson, N.E. et al. Stiffening of individual fibrin fibers equitably distributes strain and strengthens networks. *Biophys. J.* **98**, 1632-1640 (2010).

## **Acknowledgements**

This work was supported by EU programs “Thema-CNT”, “Nanopack”, “Smartpower”, “Nanotec”, “Nanocom”, “Nanoteg”, “Mercure”, and the Swedish National Science Foundation (VR) under the project “on-chip cooling using thermo-electrical device with the contract no: 2009-5042. This work was also carried out within the Sustainable Production Initiative and the Production Area of Advance at Chalmers. Y.Z. and J.L. also acknowledges the support from the Chinese Ministry of Science and Technology for the International Science and Technology Cooperation program of China (No.2010DFA14450). Y.F. also thanks Dr. Krister Svensson from Karlstad University, Dr. Alexandra Nafari from Nanofactory Instruments AB and Örjan Arthursson from Nanofabrication Laboratory in MC2, Chalmers University of Technology for the helpful and interesting discussions.

### **Author contributions**

Y.F., B.C and J.L. conceived the research. Y.F. and B.C. designed the experiments. Y.F. developed the fabrication process and synthesized the CNTs. B.C. and Y.F. carried out XRD characterization. Niklas Lindahl, Niclas Lindvall, Y.S. and Y.F. carried out the mechanical tests in AFM. Z.H., J.S., Yahui Zhang and Yan Zhang contributed to the design and analysis of the mechanical tests. J.B., A.M. and Y.F. carried out the Raman measurements. Y.F. performed the SEM. Z.L., L.Y. and Y.F. performed the TEM and EDX. Y.F. wrote the paper with input and revision from all other co-authors. J.L. supervised the whole project.

### **Additional information**

The authors declare no competing financial interests. Supplementary information accompanies this paper on [www.nature.com/naturematerials](http://www.nature.com/naturematerials). Reprints and permissions information is available online at <http://www.nature.com/reprints>. correspondence and requests for materials should be addressed to J.L.